Experimental modeling of pressurized subglacial water flow: Implications for tunnel valley formation

Thomas Lelandais, Régis Mourgues, Edouard Ravier, Stéphane Pochat, Pierre Strzerzynski, Olivier Bourgeois

Experimental modeling of pressurized subglacial water flow: Implications for tunnel valley formation

Thomas Lelandais[1], Régis Mourgues[1], Édouard Ravier[1], Stéphane Pochat[2], Pierre Strzerzynski[1], and Olivier Bourgeois[2]

[1]Laboratoire de Planétologie et Géodynamique, CNRS, UMR 6112, Université du Maine, Le Mans, France, [2]Laboratoire de Planétologie et Géodynamique, CNRS, UMR 6112, Université de Nantes, Nantes, France

Abstract Tunnel valleys are elongated hollows commonly found in formerly glaciated areas and interpreted as resulting from subglacial meltwater erosion beneath ice sheets. Over the past two decades, the number of studies of terrestrial tunnel valleys has continuously increased, and their existence has been hypothesized also on Mars, but their formation mechanisms remain poorly understood. We introduce here an innovative experimental approach to examine erosion by circulation of pressurized meltwater within the substratum and at the ice/substratum interface. We used a permeable substratum (sand) partially covered by a viscous, impermeable, and transparent cap (silicon putty), below which we applied a central injection of pure water. Low water pressures led to groundwater circulation in the substratum only, while water pressures exceeding a threshold that is larger than the sum of the glaciostatic and lithostatic pressures led to additional water circulation and formation of drainage landforms at the cap/substratum interface. The formation of these drainage landforms was monitored through time, and their shapes were analyzed from digital elevation models obtained by stereo-photogrammetry. The experimental landforms include valleys that are similar to natural tunnel valleys in their spatial organization and in a number of diagnostic morphological criteria, such as undulating longitudinal profiles and "tunnel" shapes. These results are consistent with the hypothesis that overpressurized subglacial water circulation controls the formation of tunnel valleys.

1. Introduction

The production and circulation of meltwater at the base of glaciers and their role on ice behavior and basal erosion are major issues to reconstruct the dynamics of former glacial systems on Earth. Subglacial water flow is also a key issue to predict the future behavior of the Antarctic and Greenland ice sheets in the context of the global climate change and perhaps also to assess the origin of some valleys on Mars [*Carr and Head*, 2003; *Guidat et al.,* 2015; *Souček et al.,* 2015]. When an ice sheet overlies a sufficiently permeable substratum, the meltwater infiltrates the bed and circulates as groundwater flow. Although significant amount of meltwater can be transmitted to the bed in this way [*Gooch et al.,* 2016], most models and observations agree on the inefficiency of the subglacial bed to drain all the meltwater and demonstrate that excess meltwater must circulate at the ice/bed interface [*Piotrowski,* 1997; *Breemer et al.,* 2002; *Moeller et al.,* 2007; *Lemieux et al.,* 2008]. Indeed, the innefficient groundwater drainage is counterbalanced by the formation of drainage pathways such as channels, canals, and tunnel valleys. In general, drainage systems carved into the glacier sole (R-channels) [*Röthlisberger,* 1972] develop preferentially on low-permeability bedrocks, while drainage systems carved into the bed develop preferentially on permeable beds (N-channels) [*Nye and Frank*, 1973]. This difference is illustrated, for instance, by the respective distributions of eskers and tunnel valleys below the former Fennoscandian and Laurentide ice sheets: eskers predominate on crystalline bedrocks while tunnel valleys are abundant in sedimentary basins [*Clark and Walder,* 1994].

Tunnel valleys are amongst the most spectacular landforms related to subglacial water flow, and they play a substantial role in the subglacial hydraulic system [*Boulton et al.,* 2007; *Piotrowski et al.,* 2009].

Tunnel valleys are elongated and overdeepened hollows, up to hundreds of kilometers long, several kilometers wide and hundreds of meters deep, and their formation is generally attributed to subglacial meltwater erosion [*Ó Cofaigh,* 1996; *Huuse and Lykke-Andersen,* 2000]. They are generally exposed at the emplacement of former ice sheet margins [*Jentzsch,* 1884; *Ghienne and Deynoux,* 1998; *Ehlers and Linke,* 1989; *Huuse and Lykke-Andersen*, 2000; *Le Heron et al.,* 2004; *Le Heron,* 2007]. A few examples of

subglacial tunnel valleys have also been hypothesized to exist on Mars [*Kargel and Strom*, 1992; *Head and Pratt*, 2001; *Carr and Head*, 2003; *Guidat et al.,* 2015; *Souček et al.,* 2015]. The development of tunnel valleys has strong glaciodynamic implications, as their formation may secure the stability of ice sheets by reducing water pressures at the ice/bed interface, thereby preventing catastrophic surges and ice sheet collapses [*Marczinek and Piotrowski*, 2006]. There is still no consensus, however, on the formation processes of tunnel valleys because the involved mechanisms are specific to the substratum configuration, the subglacial topography, the meltwater production rates, and the drainage characteristics [*Boulton and Hindmarsh*, 1987; *Piotrowski*, 1994, 1997; *Shaw*, 2002; *Praeg*, 2003; *Janszen et al.,* 2012; *Ravier et al.,* 2014, 2015].

Based on numerical modeling, seismic data analyses and field investigations, two major kinds of models of tunnel valley formation have been proposed. Both kinds agree on the dominant action of subglacial meltwater on tunnel valley formation, but they differ in the details of the involved mechanisms and in the time required to carve the valleys. In the first kind (steady state models), tunnel valleys form progressively in response to erosion and deformation of a soft substratum evacuated through subglacial pipes [*Boulton and Hindmarsh*, 1987] while, in the second kind (catastrophic models), they form rapidly in response to the release of considerable amounts of meltwater during outburst floods [*Piotrowski*, 1994; *Shaw*, 2002, 2010; *Hooke and Jennings*, 2006]. A specific kind of catastrophic model has been developed recently, whereby tunnel valleys form by hydraulic fracturing related to the development of fluid overpressures in a layered soft substratum [*Janszen et al.,* 2012; *Ravier et al.,* 2014, 2015]. In all these models, the formation of tunnel valleys depends on the interplay between meltwater flow evacuated at the ice-bed interface and meltwater discharged as groundwater flow.

Direct observations of tunnel valley formation processes are virtually impossible because modern subglacial environments are generally not accessible. Hence, to constrain these processes, the groundwater drainage beneath ice sheets and its implications on meltwater circulation in subglacial channels have been abundantly simulated numerically, under a wide range of input parameters [*Boulton et al.,* 1993, 2007; *Piotrowski*, 1997, 2009; *Breemer et al.,* 2002; *Lemieux et al.,* 2008; *Bense and Person*, 2008; *Person et al.,* 2012; *Flowers*, 2015]. By contrast, physical modeling is largely underrepresented in the study of subglacial meltwater flow because of the difficulty to recreate the subglacial conditions experimentally. *Catania and Paola* [2001] simulated the formation of subglacial meltwater drainage networks experimentally, by injecting pressurized water into a permeable, erodible, and noncohesive substratum covered by a rigid and transparent lid. In these experiments, braided networks formed at the substratum/lid interface, with a higher braiding intensity and a higher variability of flow directions compared to those formed under free-surface conditions. Though they did not directly address the subglacial environment, *Marra et al.* [2014] also studied experimentally the erosional effects of pressurized groundwater flow in a free-surface erodible and permeable substratum: different groundwater pressures in the substratum resulted in distinct storage and outflow processes, thus leading to various valley shapes.

Here we set the basis for a new experimental approach by developing an analog model that simulates water flow and erosion in subglacial environments. Following *Catania and Paola* [2001] and *Marra et al.* [2014], we simulate pressurized water flow by injecting pure water in a permeable and erodible sand substratum. In contrast to *Catania and Paola* [2001], however, we simulate the viscous and impermeable ice cover with a deformable and impermeable centimeter-thick cap composed of viscous silicon putty.

To provide a basis for validating the experiments, we first review the morphological characteristics of natural tunnel valleys in section 2. In section 3, we describe the experimental apparatus, the scaling of the experiments, the stereo-photographic monitoring device used to produce images, and digital elevation models (DEMs) of the experiments, and the procedure we use for the morphological analysis of the experimental valleys. The results are described in section 4. In section 5, we compare the shape and the spatial organization of experimental and natural tunnel valleys, and we discuss the implications of our results on the formation processes of tunnel valleys.

2. Morphological Characteristics of Tunnel Valleys

Tunnel valleys are elongated hollows that are generally found close to ice sheet margins. Although some examples exist on crystalline bedrocks, most tunnel valleys are carved into soft or lithified sediments

[*Grube*, 1983; *Ó Cofaigh,* 1996; *Tournier et al.,* 2010; *Janszen et al.,* 2012; *Ravier et al.,* 2014]. They are generally parallel to ice flow direction and display radial distributions. They can occur as single rectilinear to slightly sinuous segments. They can also be part of dendritic, anastomosed, or braided networks with possible cross-cutting relationships between single channels [*Paterson*, 1994; *Piotrowski*, 1997; *Huuse and Lykke-Andersen*, 2000; *Shaw*, 2002, 2010; *Praeg*, 2003; *Fisher et al.,* 2005; *Lonergan et al.,* 2006].

Their transverse profiles can be U shaped, V shaped, or box shaped [*Huuse and Lykke-Andersen*, 2000; *Jørgensen and Sandersen*, 2006]. Morphometric analyses based on boreholes, seismic data, and outcrop observations reveal that their flanks are steep (12–32° for Pleistocene tunnel valleys in the North Sea [*Kristensen et al.,* 2007], 10–25° for Ordovician tunnel valleys in North Africa, [*Le Heron et al.,* 2004; *Clerc et al.,* 2013], and sometimes almost vertical [*Piotrowski and Tulaczyk*, 1999; *Le Heron et al.,* 2004; *Kristensen et al.,* 2007]).

One morphological characteristic generally considered as diagnostic of tunnel valleys is their constant width along their paths. This has been observed, for instance, in the central and eastern North Sea [*Stewart et al.,* 2013; *Kristensen et al.,* 2007], in Alberta, Canada [*Atkinson et al.,* 2013], and at the Kalamazoo River Valley, Michigan, USA [*Kozlowski et al.,* 2005]. Tunnel valleys with varying widths have been described however in North America [*Livingstone and Clark*, 2016].

The average width/depth ratio of tunnel valleys is close to 10:1 [*Ghienne and Deynoux*, 1998; *Gibling*, 2006; *van der Vegt et al*, 2012]. However, this ratio is highly variable because it is controlled by different parameters such as the substratum properties (erodability and permeability) and the hydraulic gradient controlled by the ice thickness. The resistance of the substratum to erosion has been identified to control their size, spacing, and width/depth ratio [*Woodland*, 1970*; Moores,* 1989]. For example, tunnel valleys incised in chalk are narrower than those incised in unconsolidated bedrocks [*Praeg,* 2003*; Moreau et al.,* 2012].

A diagnostic characteristic of tunnel valleys is their abrupt upstream and downstream terminations (upstream and downstream referring to the ice flow direction) [*Moores*, 1989; *Wingfield*, 1990; *Ó Cofaigh,* 1996; *Lonergan et al.,* 2006]. They generally begin and end randomly with no connection to any obvious catchment basin or drainage network [*Eyles and de Broekert*, 2001; *Lowe and Anderson*, 2003], and the longitudinal slopes of their upstream and downstream terminations range between 1° and 13° [*Kristensen et al.,* 2008; *Moreau et al.,* 2012].

Tunnel valleys floors often display undulating long profiles, with overdeepened sections and adverse slopes [*Sjogren and Rains*, 1995]. This has been observed in many tunnel valleys worldwide, like the Thornapple valley in Michigan [*Kehew et al.,* 2013], the Quaternary Enniskerry drainage system in eastern Ireland [*McCabe and Ó Cofaigh*, 1994], the Crocodile channels in southern Alberta [*Rains et al.,* 2002], or the central North Sea tunnel valley system [*Stewart et al.,* 2013]. Since adverse slopes are difficult to reconcile with free-surface water flow, their existence is generally taken as evidence for the formation of tunnel valleys by confined and pressurized water flow [*Beaney*, 2002]. Adverse slopes also exist in subaerial fluvial systems and are related to deep scouring, which has a direct relationship with the discharge [*Latrubesse*, 2015]: deep scouring is limited to river segments where flow convergence increases the discharge [*Parsons et al.,* 2008; *Blanckaert*, 2010]. By contrast, in subglacial tunnel valleys, adverse slopes can occur repeatedly along valley paths whatever the discharge and with no connection to flow convergence [*Stewart et al.,* 2013]. This specific characteristic is thus one of the most valuable diagnostic criteria to discriminate tunnel valleys from fluvial valleys [*Ó Cofaigh,* 1996].

3. Analog Modeling

3.1. Experimental Apparatus

The experimental apparatus consists of a glass box (70 cm long, 70 cm wide, and 5 cm deep). A 5 cm thick substratum composed of sand with an average grain size of 100 μm, saturated with pure water, rests on the box floor, and is partially covered with a circular ($r_1 = 15$ cm), 3 cm thick ($h_{silicon}$), impermeable and viscous ($\eta = 5 \times 10^4$ Pa s) silicon cap (Figure 1a). Silicon putty, a viscous and impermeable material has been selected to simulate ice because its transparency allows to observe and take photographs of the experimental valleys formed at the silicon cap/substratum interface.
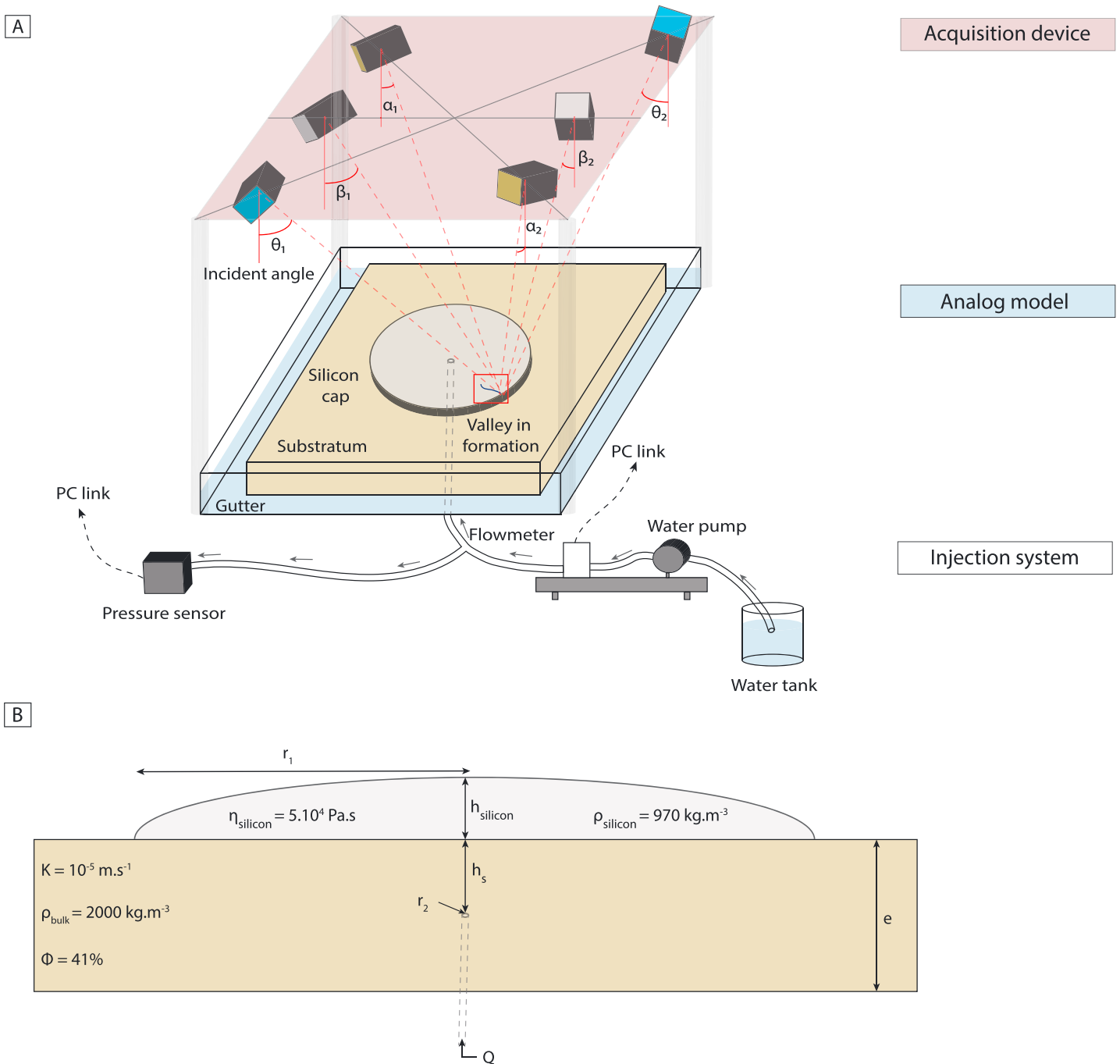
Figure 1. Experimental apparatus. (a) Acquisition device, analog model, and water injection system. Grey arrows symbolize the water flow direction. The photographic device is composed of three pairs of cameras focused on the valleys in formation. The incident angle is measured for every camera and used for the correction of the digital elevation model. (b) Transverse section of the analog model and associated variable and parameters.

The substratum is compacted to ensure homogeneous values for its density ($\rho_{bulk} = 2000 \, \text{kg m}^{-3}$), porosity ($\Phi = 41\%$), and permeability ($K = 10^{-5} \, \text{m s}^{-1}$) (Figure 1b). For technical reasons, the deposition of the silicon cap during the preparation of the experiments leads to the formation of a central depression, 0.1 to 1 mm in depth, 15 to 30 cm in diameter, bordered by a marginal ridge, at the substratum/silicon interface (Figure 3). The depression and its marginal ridge exist at the onset of all experiments and thus simulate a pre-existing topography at the ice/substratum interface.

Water discharge below the silicon cap is achieved by a punctual injector ($r_2 = 4\,$mm) placed at the model center, at a depth of 1.5 cm (h_s) below the substratum/silicon interface, and connected to a pump, a flowmeter and a pressure sensor (Figure 1a). The pressure sensor records the water pressure evolution in the injection system, at the injector altitude (1.5 cm below the substratum/silicon interface) during the whole experiment.

The experimental setup reproduces a confined aquifer with a circular boundary, where water flow and pressure can be calculated with the Dupuits analytical solution (equation (1)). The implemented water discharge (Q) is thus calculated beforehand using this solution which takes into consideration the silicon thickness and radius and the differential pressure between the silicon cap center and its margin converted in water height. The water discharge injected in the system (Q) is modulated with the pump to obtain a water pressure at the injector close to the sum of the glaciostatic and lithostatic pressures (respectively inferred from the silicon and sand weight) (equation (1)):

$$Q = \frac{2\pi K e \frac{P_{water}}{\rho_{water}\,g}}{\ln\left(\frac{r_1}{r_2}\right)} \tag{1}$$

with $P_{water} = (\rho_{bulk}\,g\,h_s) + (\rho_{silicon}\,g\,h_{silicon})$ expressing the water pressure corresponding to the sum of glaciostatic and lithostatic pressures and $r_1 =$ radius of silicon cap (m); $r_2 =$ radius of injector (m); $e =$ sand thickness (m); $K =$ permeability (m s^{-1}); $h_{silicon} =$ silicon thickness (m); $h_s =$ sand thickness above the injector (m); $\rho_{bulk} =$ density of the sand (kg m^{-3}); $\rho_{silicon} =$ density of the silicon (kg m^{-3}), and $\rho_{water} =$ density of the water (kg m^{-3}) (Figure 1b).

3.2. Scaling

The potentiometric surface of groundwater in a subglacial confined aquifer is parallel to the ice surface, therefore implying that water pressure diminishes toward the ice margin [*Fountain and Walder*, 1998]. Thus, the position of the ice margin, subject to fluctuations through time, controls groundwater flow characteristics in glacial settings. Similarly, in our experiments, the silicon putty margin controls the water pressure gradient. In this perspective, we base the scaling on the displacement of the natural ice and experimental silicon margins through time. For that purpose, we determine a speed ratio (γ) corresponding to the ratio between the margin velocity and the incision rate required to form a tunnel valley. We compare the value of this dimensionless ratio in natural examples (γ_{nat}) with its value in the experiments (γ_{exp}). Ideal scaling requires that γ_{exp} is equal to γ_{nat}.

Considering the variability in depths of natural and experimental tunnel valleys, we define natural (subscript nat) and experimental (subscript exp) incision rate ranges using the depth of the valleys (h):

$$h_{nat} = 10^2 \text{ m to } 5 \times 10^2 \text{m}$$
$$h_{exp} = 5 \times 10^{-1} \text{mm to } 2 \times 10^0 \text{mm}$$

and an estimation of the time range required to form experimental and tunnel valleys (t):

$$t_{nat} = 10^2 \text{ years to } 10^4 \text{ years}$$
$$t_{exp} = 10^2 \text{ seconds to } 10^3 \text{ seconds.}$$

Using theses ranges, we are able to determine experimental and natural incision rate ranges ($v_{incision}$).

$$V_{incision\_nat} = 10^{-2} \text{m/year to } 5\text{x}10^0 \text{m/yr}$$
$$V_{incision\_exp} = 3.15 \times 10^1 \text{ m/yr to } 6.3 \times 10^2 \text{m/yr.}$$

The speed of natural glacier margins (V_{ice}) ranges between $10^{-1}\,$m/yr for stable glaciers and $10^3\,$m/yr (cf. Figure 1) the maximal speed observed during glacial surges [*Dowdeswell et al.,* 1991; *Björnsson et al.,* 2003; *Solomina et al.,* 2016]. In our experiments, silicon cap is driven by gravity and can only simulate margin advances. We thus focus our scaling on glaciers with positive values of margin velocities only.

The speed of the silicon cap margin ($V_{silicon}$) in the experiments is always positive and is comprised between $10^{-2}\,$mm/s and $10^{-1}\,$mm/s. The experimental speed ratio (γ_{exp}) is therefore comprised between 0.5 and 100 (Figure 2). Using the natural values for the incision rate and the margin velocity, we delineate
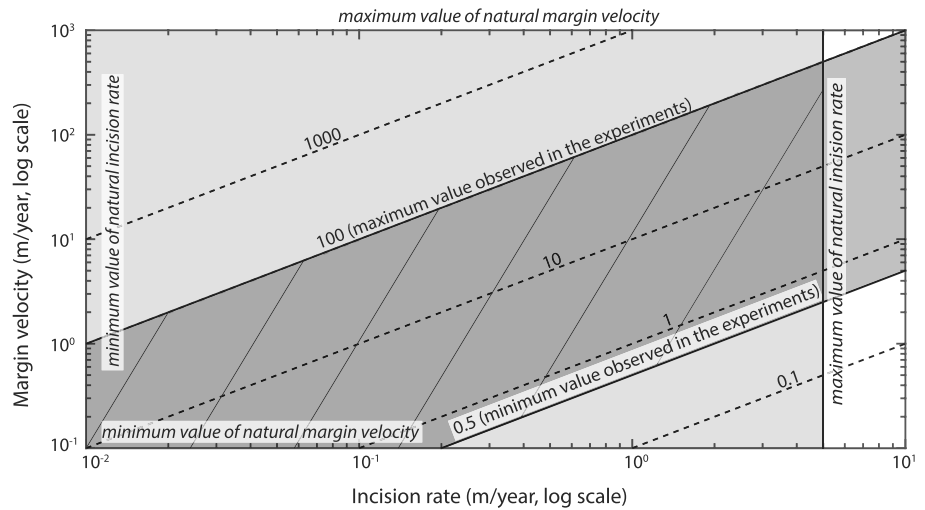
Figure 2. Value of speed ratio (dashed lines) as a function of natural incision rate and natural margin velocity. Light-shaded box: field of possible natural margin velocities (0 to 1000 m/yr) and incision rates (0.01 to 5 m/yr). Dark-shaded polygon: field of validity of the experiments, defined by the minimal (0.5) and maximal speed ratios observed in the experiments. Hatched polygon: the overlap between the light-shaded box and the dark-shaded parallelogram defines the range of natural settings that we can reproduce experimentally.

a field of possible natural margin velocities and incision rates (cf. light-shaded box in Figure 2). The projection of the minimal and maximal experimental speed ratios highlights the field of validity of the experiments and defines the range of natural settings we can reproduce experimentally (cf. hatched polygon in Figure 2).

3.3. Postprocessing

During the experiments, surface images are collected by six synchronized cameras, which take photographs simultaneously every 5 s, from a distance of 1 m above the box (Figure 3a). DEMs and orthophotographs of the experiments are generated from these photographs with the Agisoft Photoscan© photogrammetry processing software.

Light refraction in the silicon cap, however, induces vertical and lateral offsets between the real and measured positions of points at the cap/substratum interface. The topographic reconstruction using photographs taken through the refractive silicon thus requires a correction. We developed a two-step correction procedure based on the orientation of the photographs and the refractive properties of the silicon putty
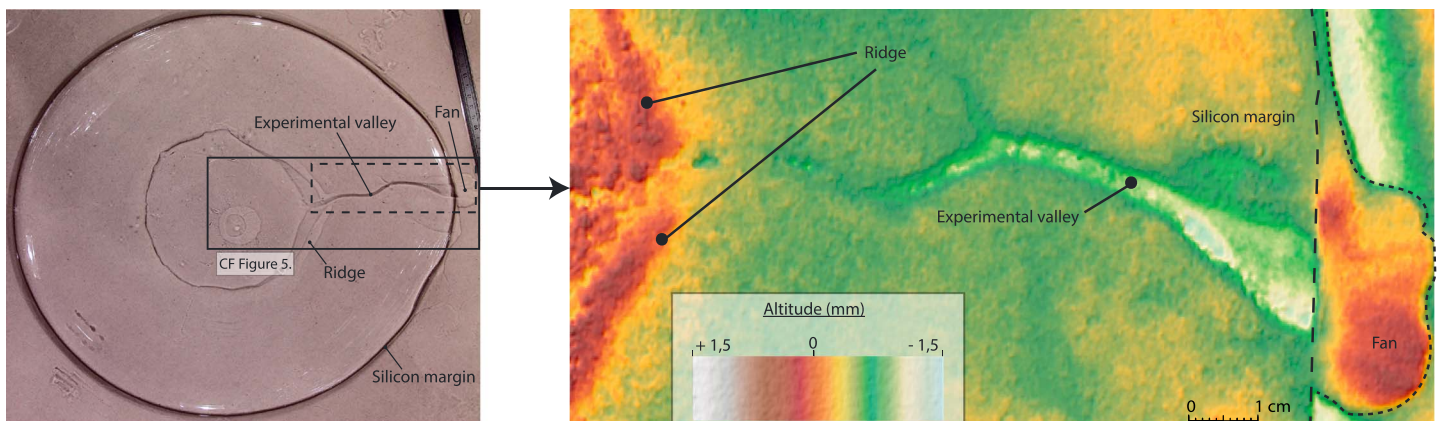

Figure 3. Surface photograph of an experiment and DEM of an experimental valley produced by stereo-photogrammetry.

(supporting information). In the first step, the thickness of the silicon cap is computed and interpolated from its elevation measured at a set of references points where the elevation of the substratum is 0. In the second step, using this interpolated thickness and the incident angle of every camera, the vertical offsets between the measured positions of points located below the silicon cap and their real positions are estimated. Preliminary tests performed on objects with known topographies show that the average error after the acquisition and the correction is about 10% on the retrieved elevations.

3.4. Morphological Analysis

To analyze the shape of the experimental valleys from the reconstructed DEMs and orthophotographs, we designed a custom MATLAB code. After a first step of manual digitization of valley bottoms and edges on the DEMs and orthophotographs (Figures 4a and 4b), the algorithm automatically plots a series of transverse profiles at regular intervals (Figures 4c and 4d). Valley widths and depths are measured along these profiles, using the positions and elevations of the intersections between the automatically extracted cross sections and the manually extracted valley edges (Figure 4e). Valley widths at half depth and at quarter depth [*Graveleau and Dominguez*, 2008] and average slope gradients of valley flanks are also extracted. Valley floor long profiles are measured along the valley axis, defined as the line passing through the points of minimal elevation of every transverse profile (Figure 4f). A sinuosity index is calculated by dividing the curvilinear length of the valley axis (measured as the cumulated lengths of all its segments) by its rectilinear length (measured as the distance between its first and last points).

4. Experimental Results

We conducted 15 experiments with various input parameters. All the experiments lead to different results because their dynamics were controlled by a complex combination of variable physical parameters including viscosity of the silicon putty and water, roughness, or microtopography of the substratum, sand compaction, and permeability heterogeneities in the substratum. We discuss here in details the results of seven representative experiments, for which we obtained good-quality DEMs (Table 1).

4.1. Progress of Experiments

Four major stages in the processes of valley formation are observed in all experiments.

1. As long as the water pressure remains below the sum of the glaciostatic and lithostatic pressures (Figure 5a), the silicon cap margin migrates outward at a regular rate, in response to viscous internal deformation of the silicon. The only topographic features visible at the silicon/substratum interface are the preexisting central depression and its marginal ridge. No drainage landform appears at this interface because the water circulation occurs as groundwater flow only.
2. Once the water pressure exceeds the sum of the glaciostatic and lithostatic pressures (Figure 5b), the sand layer above the injector is fluidized, and water starts to flow at the silicon-substratum interface. The pressure threshold is significantly larger than the sum of glaciostatic and lithostatic pressures because of pressure dissipation within the permeable substratum as a consequence of lateral water flow during vertical injection. The onset of fluidization is marked by a drop in the water pressure curve. Microtopographic features form at the interface, such as sand accumulations and incipient microvalleys. The microvalleys initiate suddenly by remobilization and evacuation of sand by water flowing at the interface. They form simultaneously at different locations along the silicon cap margin, in response to the radial water flow induced by the experimental setup.
3. Following this initial fluidization and remobilization stage, the water pressure stabilizes in response to the injection of a constant water discharge into the system (Figure 5c). Decoupling due to water overpressure at the substratum/silicon interface accelerates the motion of the silicon cap. The formation of the microtopographic features creates local high permeability zones, responsible for the development of local pressure gradients in the substratum (Figure 5b). These pressure gradients lead to the convergence of water flow toward the incipient valleys. Major changes are observed in the drainage network, which turns into a system of well-developed and delineated valleys.
4. As the experiment continues, the valley dimensions and shapes continuously evolve and their heads migrate backward by regressive erosion, until they eventually reach the central topographic depression and the injector (Figure 5d). Some valleys and tributaries are occasionally filled by sand and abandoned,

I. Manual digitization
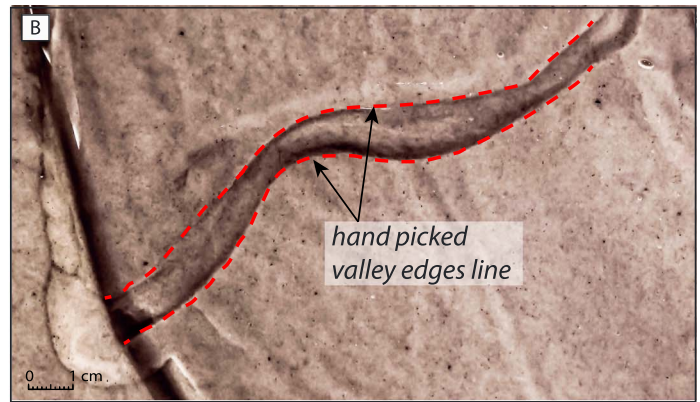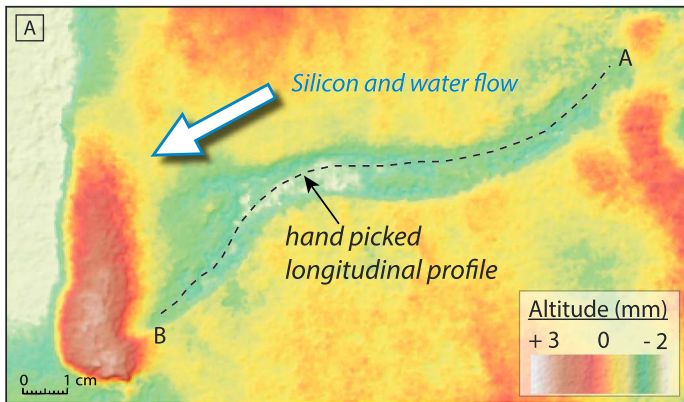
II. Generation of cross-sectional profiles
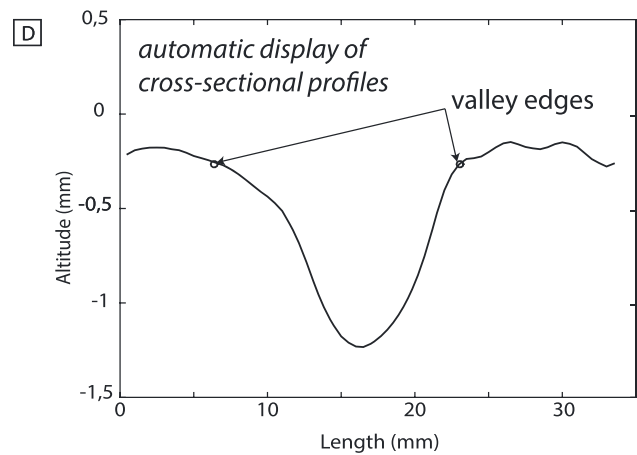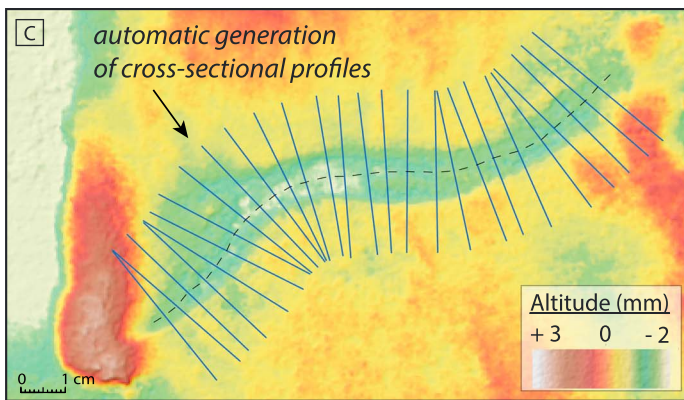
III. Morphological database creation (valley width, depth, flank slope and axis position)
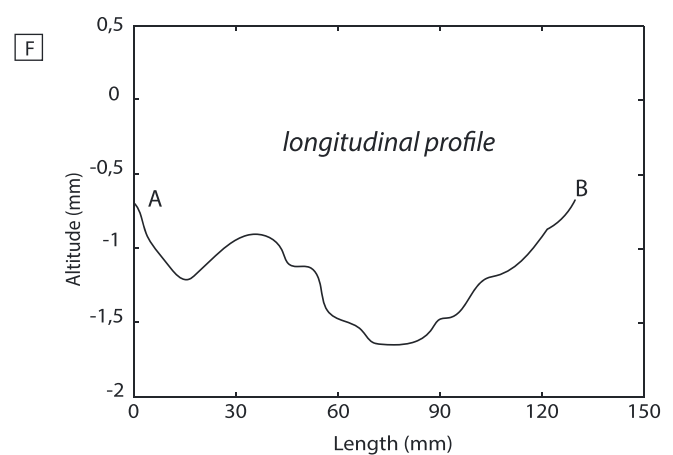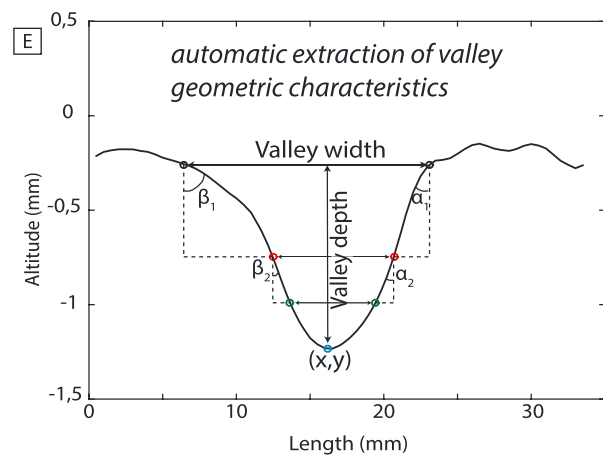
Figure 4. Principle of the morphological analysis of experimental valleys. (a) Manual digitization of valley axis on DEM. (b) Manual digitization of valley edges on orthophotographs. (c) Automatic generation of cross-sectional profiles along the valley axis. (d) Automatic display of every cross-sectional profile and valley edges. (e) Automatic extraction of the geometric data. Valley widths are measured between valley edges. Valley depths are measured between valley edge altitudes and the minimal altitude of the transverse profiles. Half-depth and quarter-depth widths are automatically calculated from valley depths and widths. Valley flank slopes ($\alpha 1$, $\alpha 2$, $\beta 1$, and $\beta 2$) and valley axis position and altitude are automatically extracted. (f) Valley bottom longitudinal profiles are plotted from the altitude of the points previously extracted.

Table 1. Summary of Input Parameters and Results for Seven Selected Experiments[a]

Experiment Number	Injection Discharge (mL/h)	$h_{silicon}$ (mm)	R_1 (mm)	Valley Number	Length (mm)	Average Width (mm)	Average Depth (mm)	Width/Depth Ratio	Average Slope of Left Flank (deg)	Average Slope of Right Flank (deg)	Slope of Upstream and Downstream Terminations (deg)	Sinuosity Index	Dominant Cross-Sectional Shape
1	1500 to 3000	30	15	1	133.7	11.1	1.2	9.2	20	17	9	1.05	U shaped
				2	69.0	6.8	0.7	9.67	14	14	5.2	1.02	U shaped
				3	72.5	6.9	0.3	23	9	9	2.6 and 5.9	1.02	U shaped
2	1500	30	15	4	91.8	12	0.8	15	12	9	4.5	1.15	U shaped
3				5	143.8	18.6	1.08	17.22	14	8	2.3	1.06	U shaped
4				6	91.1	9.8	0.76	12.85	11	13	3.7 and 3.2	1.05	U shaped
5	3000	30	15	7	97.7	8.0	0.64	12.49	12	14	4.4	1.03	U shaped
				8	69.3	4.8	0.39	12.17	16	19	2.8	1	U shaped
				9	59.8	5.8	0.525	11.06	17	16	7.7	1.01	U shaped
6	1500	15	15	10	113.8	7.9	0.512	15.37	16	17	3.2 and 4.2	1.06	U shaped
7	1500	30	20	11	78.1	9.6	0.741	12.96	15	12	8.3	1.02	U shaped
				12	82.8	8.7	0.693	12.5	15	12		1.02	U shaped
				13	80.3	12	1.06	11.3	16	12		1.03	U shaped

[a]Widths, depths, and flank slopes have been averaged over the total length of the valleys.

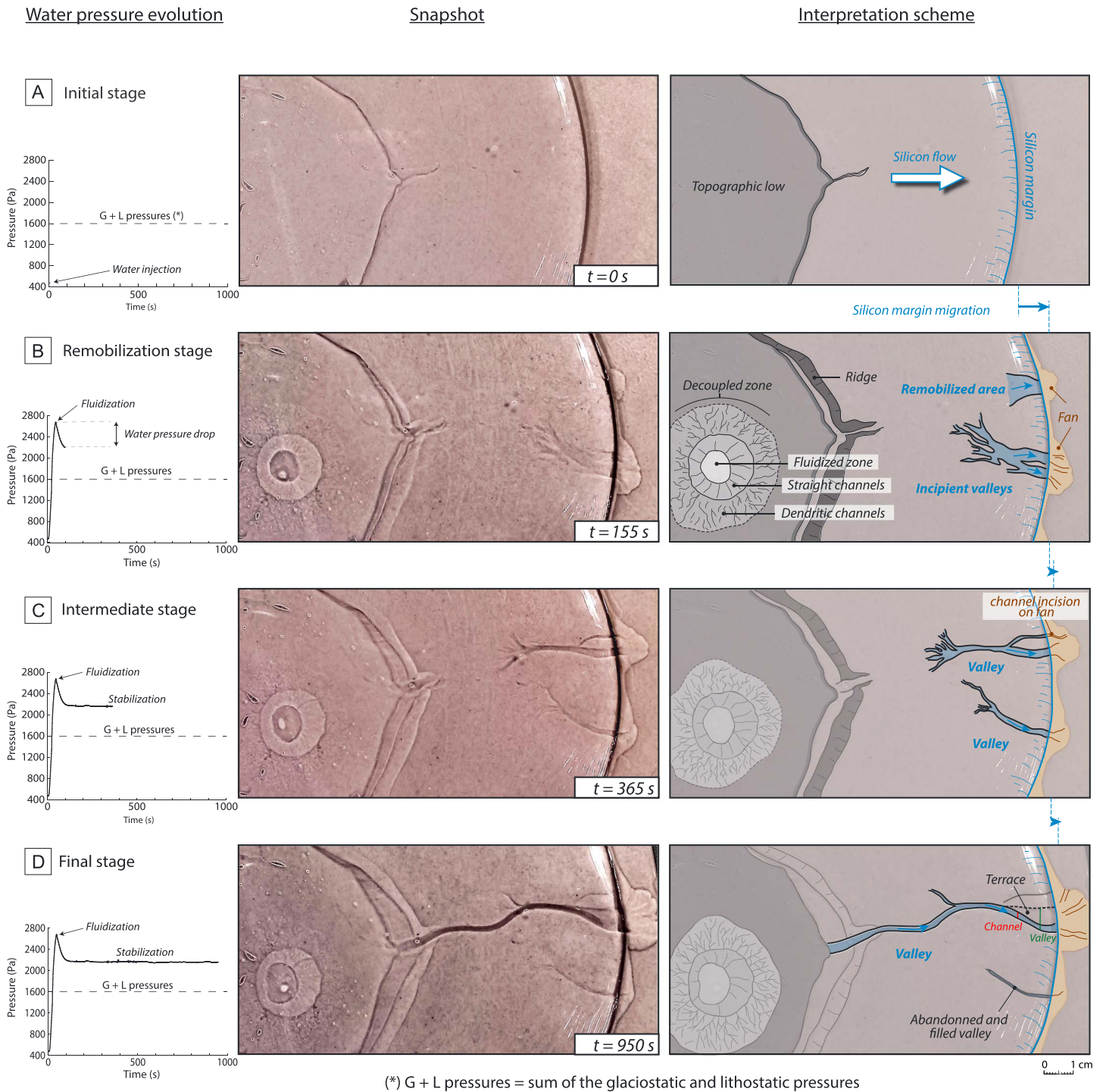(*) G + L pressures = sum of the glaciostatic and lithostatic pressures

Figure 5. The four main stages of experimental valley evolution illustrated by (from left to right) the water pressure curve, a surface view of the experiment, and its interpretative sketch. (a) Initial stage: onset of water injection. (b) Remobilization stage: formation of incipient microvalleys associated with fluidization of the substratum above the central injector. (c) Intermediate stage: evolution from incipient to well-delimited valleys. (d) Final stage: valley heads have migrated backward to the central depression and marginal fans have formed at valley mouths.

while others remain active. The wandering of some active channels leads to progressive enlargement of some valleys and formation of lateral terraces corresponding to abandoned channels. The presence of these lateral terraces allows to differentiate the channel in which water flow is active and the entire

incision referred as to the valley width (Figure 5d). Fan-shaped sand deposits form at valley mouths, along the outer side of the silicon cap margin. Rapid flow events ("surges") of the silicon cap occur occasionally in corridors located above the valleys.

4.2. Morphology and Spatial Organization of Valleys

The experimental valleys show a large range of dimensions (Table 1), with lengths ranging from 6 to 14 cm, widths ranging from 4 to 12 mm and depths ranging from 0.3 to 1.2 mm. Their long profiles show recurring overdeepenings and adverse slopes (2° to 6°, Figure 6). The experimental valleys frequently display constant channel widths (Figure 7). Their width-depth ratios range from 9 to 23, with 11–12 being the most common values (Table 1). The cross-sectional profiles are generally U shaped to box shaped, but local V-shaped profiles occur along some valley paths in association with overdeepenings (Table 1). The slope gradients of their flanks range from 8° to 20°, 15° being the most common value. Dissymmetric flanks are occasionally observed (Table 1, valley 5). Slope gradients have been measured at the heads of all valleys and at their downstream terminations when this was possible. These slope gradients are comprised between 2° and 10°. The sinuosity index ranges from 1 to 1.15, corresponding to nearly rectilinear courses.

In all the experiments, the valleys formed perpendicular to the margin of the silicon cap (i.e., parallel to the motion of the silicon) and defined radial networks. Two kinds of networks were obtained: the first kind, developed when the water discharge injected at the start of the experiment exceeded the theoretical one (cf. equation (1)) is composed of a few valleys with tributaries (Figure 8a) and, the second kind, developed when the water discharge injected corresponds to the theoretical one, is composed of nonconnected rectilinear segments (Figure 8b). In both kinds of networks, the valley heads are unclear, their catchment basins are poorly expressed in the topography, and the valleys terminate abruptly downstream, either within the extent of the silicon cap or at its margin.

4.3. Sensitivity Study

To explore how changes in the experimental parameters impact the morphology of the valleys, we conducted a sensitivity study by varying the thickness and diameter of the silicon cap and the water discharge (Table 1 and Figure 9). The reference is an experiment with $h_{silicon} = 30$ mm; $r_{silicon} = r_1 = 150$ mm; $Q = 1500$ mL/h (Figure 9a). The width-depth ratio of the valleys formed in all the sensitivity experiments is generally greater than 10:1 (Figure 9). The valleys are more numerous and shallower when the discharge is higher ($Q = 3000$ mL/h, Figure 9b) or when the silicon cap is thicker (Figure 9c). The valleys get deeper when the water discharge increases gradually than when it is constant (Figure 9d). No impact on valley dimensions is observed by varying the radius of the silicon cap (Figure 9e).

5. Discussion

5.1. Morphological Comparison Between Experimental and Natural Tunnel Valleys

5.1.1. Long Profile

All the valleys produced in our experiments have undulating long profiles with local overdeepenings and adverse slopes (Figure 6 and Table 2). Similar profiles have been identified in several natural tunnel valleys worldwide, like the Thornapple valley in Michigan [*Kehew et al.,* 2013], the quaternary Enniskerry drainage system in eastern Ireland [*McCabe and ÓCofaigh,* 1994], the Crocodile channels in southern Alberta [*Rains et al.,* 2002], or the central North Sea tunnel valley system [*Stewart et al.,* 2013]. Our experimental results are consistent with the classic interpretation that undulating long profiles of natural tunnel valleys are related to confined and pressurized subglacial water flow [*Ó Cofaigh,* 1996; *Beaney,* 2002].

5.1.2. Width

The valleys formed in the experiments frequently have constant widths along their paths (Table 2 and Figure 7). These valleys formed by progressive deepening of channels that remained stable in position through time. By contrast, valleys with varying widths were produced by channels that wandered laterally (Figure 7). Constant valley width is generally considered as a diagnostic characteristic of natural tunnel valley systems (e.g., in central and eastern North Sea) [*Stewart et al.,* 2013; *Kristensen et al.,* 2007], but examples of tunnel valleys with varying widths have been described in North America [*Livingstone and Clark,* 2016]. Based on our experimental results, we infer that natural tunnel valleys are constant in width when subglacial
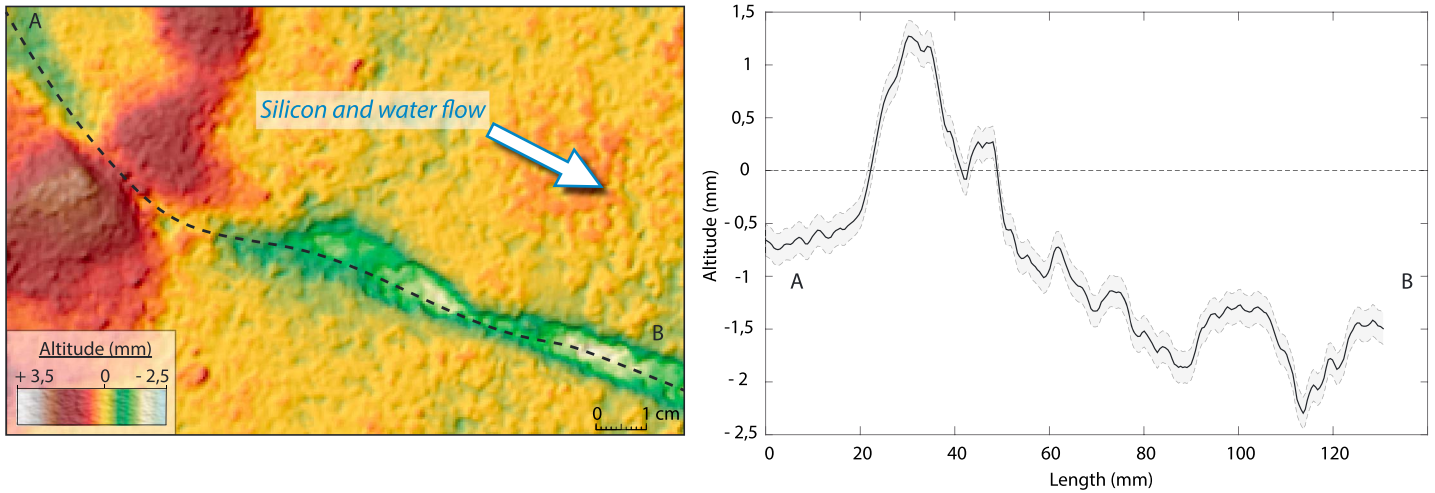
Figure 6. Example of an experimental valley with an undulating long profile. The shaded strip along the profile symbolizes the error on the elevation measurements.

meltwater channels remain stable in position through time, while tunnel valleys with varying widths form when these channels wander laterally.

5.1.3. Width-Depth Ratio

The width/depth ratio of valleys is a classical morphological index and is often used to differentiate tunnel valleys from other glacial incisions [*Ghienne and Deynoux*, 1998]. Both in our experiments and in nature, the average value of this dimensionless ratio is about 10:1 (Figure 10 and Tables 1 and 2). This statistical relation seems to be independent of the water discharge, the pressure, and the silicon cap geometry (Figure 9). A wider variability of this ratio is observed in natural tunnel valleys than in our experiments, however, which can be attributed to the influence of the substratum lithology [*Ghienne and Deynoux*, 1998; *Kristensen et al.*, 2008; *van der Vegt et al.*, 2012; *Stewart et al.*, 2013].

5.1.4. Cross-Sectional Morphology

The experimental valleys display U-, V- and box-shaped cross-sectional shapes, often with steep flanks (12 to 18° on average, with maximal values of about 30°) and flat or curved floors (Figure 11 and Tables 1 and 2). Terraces and dissymmetric valley flanks are obtained in some experiments where the channels wandered

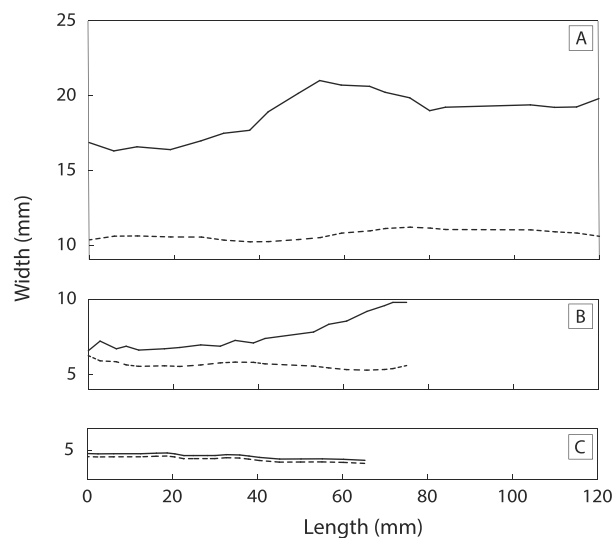**Figure 7.** Width of three selected valleys (plain lines) and their associated channels (dashed lines) plotted against distance from valley heads. (a) Valley width increases in its central section, while channel width remains constant. (b) Valley width increases at the margin of the silicon cap, while channel width remains constant. (c) Valley and channel widths are identical and remain constant.
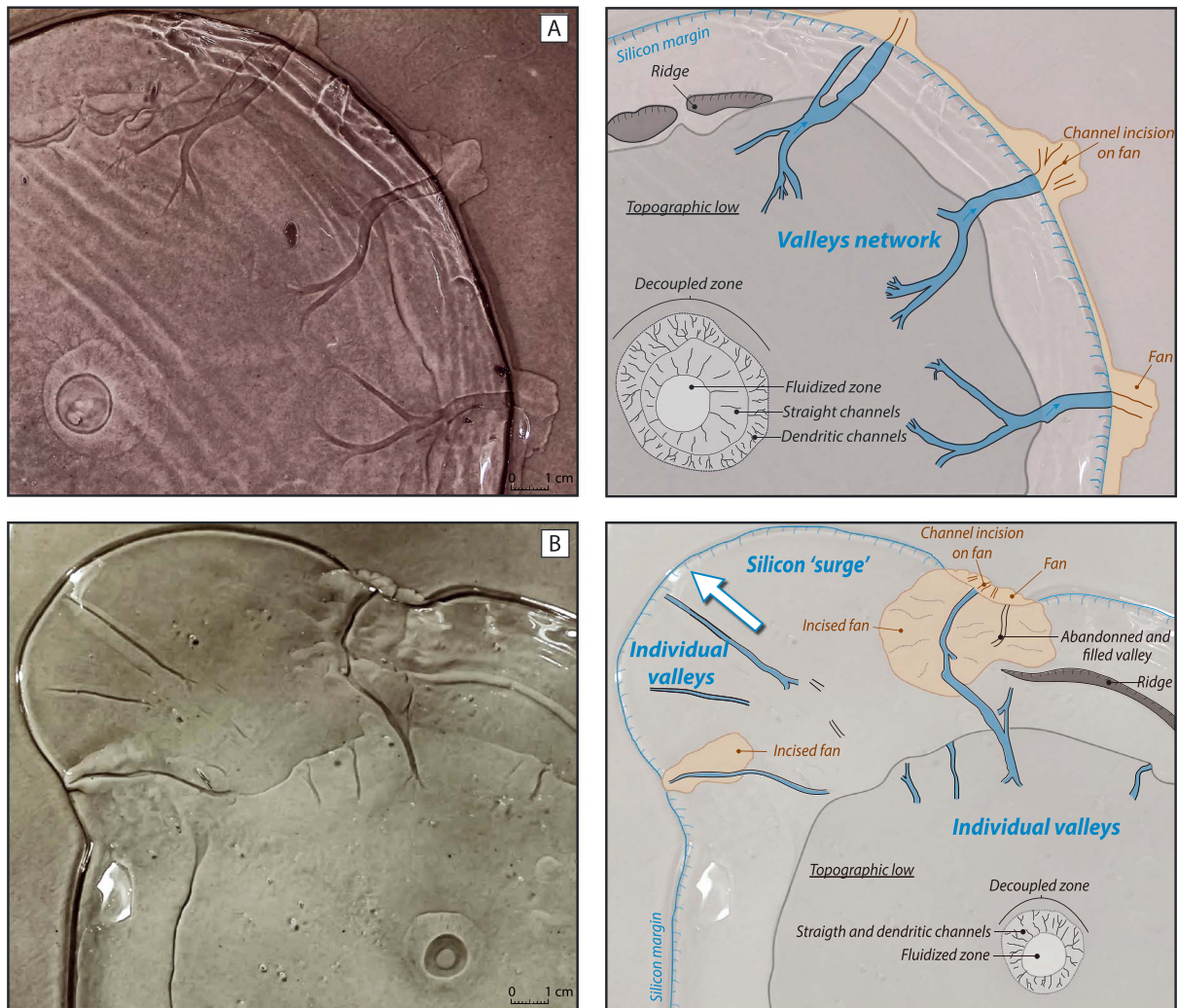
Figure 8. Examples of experimental drainage networks. (a) Radial tributary networks. (b) Individual valleys organized radially and associated with a silicon surge. Note the correlation in location and direction between the silicon surge and the valleys.

laterally. The cross-sectional shapes of the experimental valleys are thus in agreement with those of natural tunnel valleys (Figure 11).

5.1.5. Upstream and Downstream Terminations

The experimental valleys display upstream and downstream terminations slopes ranging from 2 to 9° with mean values around 5–8° (Table 2). They also seem, in some cases, to begin randomly and their catchment basins are not visible in the topography. These values and observations are consistent with natural tunnel valley upstream and downstream terminations.

5.1.6. Subglacial Drainage Patterns

The experimental valleys display two major kinds of drainage patterns: network comprised of individual (Figure 8b) and tributary networks (Figure 8a), related to low water discharge and high water discharges, respectively. Water discharge being closely link to water pressure, experimental valleys displaying a spatial organization with adjacent tributaries have formed under higher water pressures. Higher water pressures might increase the area of silicon-substratum decoupling and therefore promote the development of larger drainage zones at the interface. Based on these results, we infer that tributary networks might form below extensive zones of ice-bed decoupling allowing a widespread drainage network to develop. Conversely, individual tunnel valleys might form below localized zones of ice-bed decoupling related to lower porewater pressures.
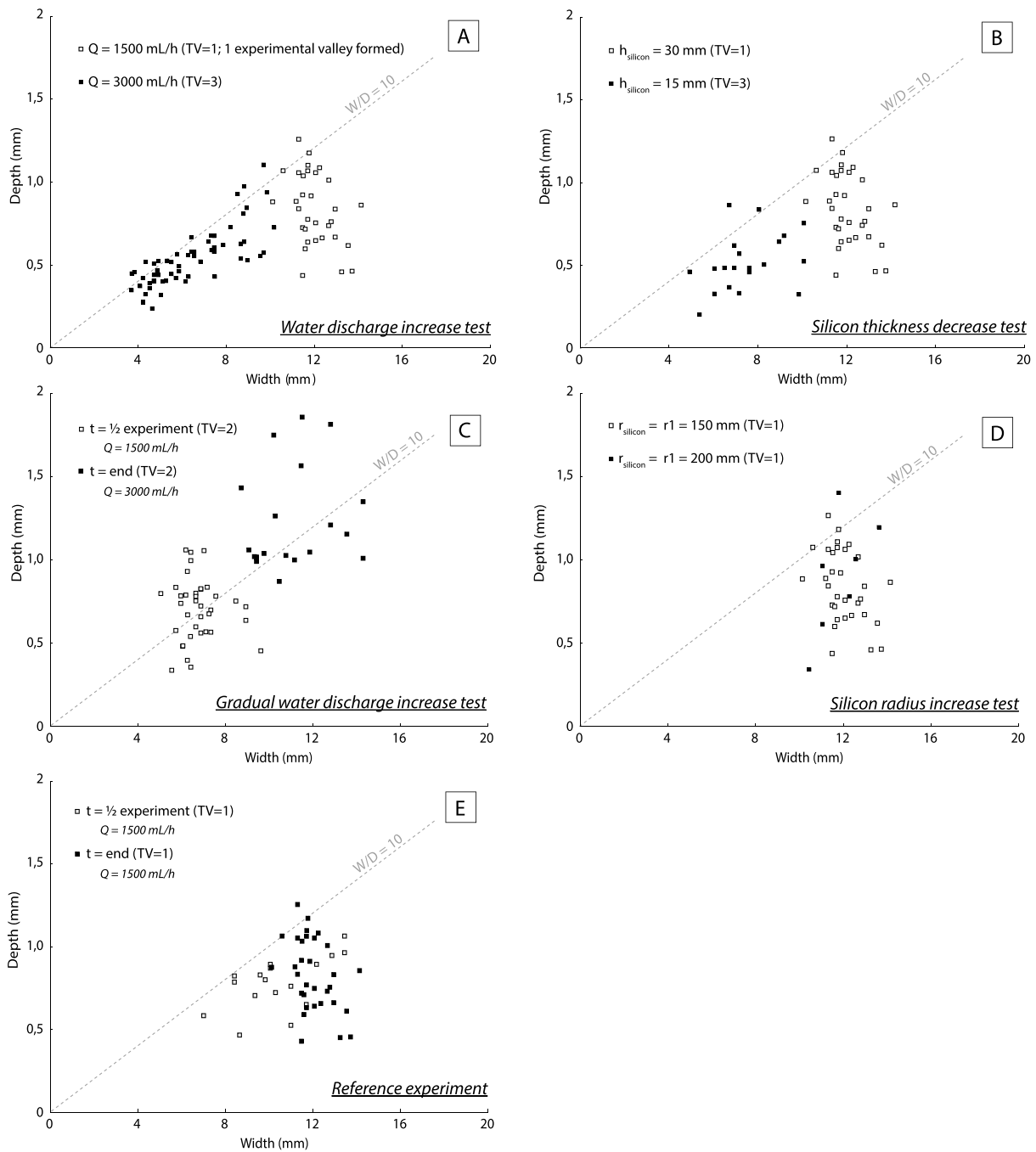
Figure 9. Dimensions (widths and depths) of valleys formed in five different experiments. In each experiment, one parameter has been modified with respect to a reference experiment. Reference experiment: $h_{silicon} = 30$ mm; $r_{silicon} = r_1 = 150$ mm; $Q = 1500$ mL/h. In the (a) water discharge increase test, a higher constant discharge is similar to water pressure increase since discharge is linked to water pressure. In the (b) silicon cap thickness test, a decrease of silicon thickness without modifying water discharge is similar to an increase of water pressure. In the (c) gradual water discharge increase test, water discharge, is gradually increased from 1500 mL/h to 3000 mL/h. (d) In the (d) silicon cap radius increase test, the diameter of the silicon has been set to 40 cm. In the (e) reference experiment water discharge is maintained at 1500 mL/h during the whole experiment.

However, natural tunnel valley networks can be much more complex and differ from the experimental results. The variability of tunnel valleys spatial organizations could result of parameters impossible to recreate such as a fluctuating ice margin positions through time or overlaps of multiple incisions related to ice sheet advances or retreats [*Kristensen et al.*, 2007; *Sandersen et al.*, 2009; *Stewart and Lonergan*, 2011].

Table 2. Comparison of Experimental and Tunnel Valleys Characteristics (Modified From *van der Vegt et al.* [2012])

Criteria	Characteristics of Natural Tunnel Valleys	Characteristics of Experimental Tunnel Valleys
Location	Found within boundaries of former ice sheets Parallel to ice sheet movement/Perpendicular to ice sheet margin Commonly found on erodible substratum (sand, silt, clay, till, limestone, and chalk)	Found within boundaries of silicon cap Parallel to silicon cap movement/Perpendicular to silicon cap margin Erodible substratum (saturated sand)
Morphology	Over 100 km long (1–40 km segments typically) Maximum 5 km wide (500–1500 m typically) Maximum 400 m deep (20–200 m typically) Width-depth ratio. 1:10 U- and V- shaped valleys, U-shaped most common Steep flanks, 20–25° most common Upstream termination slope: 1–6° most common, 13° max Downstream termination slope: 1–6° most common, 11° maximum Slightly sinuous courses Undulating long profiles with overdeepenings and adverse slopes	Over 15 cm long (8–10 cm typically) Over 2 cm wide (0,8–1 cm typically) Maximum 2,5 mm deep (1–1,5 mm typically) Width-depth ratio average. 1:10 U- and V-shaped valleys, U-shaped most common Gentle to steep flanks, 11–12° most common, 30° max Upstream termination slope: 5–8° most common, 9° max Downstream termination slope: 4–6° most common, 9° maximum (lack of measurements) Slightly sinuous courses (sinuosity index less than 1,1) Undulating long profiles with overdeepenings and adverse slopes
Network	Single channels, anastomosing networks, crosscutting relationships, channels reuse	Single channels, tributary networks, radial networks, channels reuse

5.2. Proglacial Fans Associated With Tunnel Valleys

In the experiments, fan-shaped accumulations form at the margin of the silicon cap by deposition of sand particles that were extracted from the substratum below the silicon cap and exported along the valleys. Channel networks are observed on these fans, which thus resemble natural proglacial fans [*Bennett et al.,* 2002; *Winsemann et al.,* 2007]. In the experiments, the fans play a substantial role in the evolution of the valleys and in the motion of the silicon cap: as the valleys grow, the fans widen and thicken until they form obstacles and deviate both the silicon and the water flow (Figure 8). Similarly, proglacial fans located at the mouth of natural ice-streams have been hypothesized to induce ice-grounding and back-stress stopping, potentially responsible for deceleration and deviation of ice streams [*Thomas et al.,* 1988; *Bennett,* 2003].

5.3. Relations Between Valley Orientation and Ice Flow

The experimental valleys initiate close to the margin of the silicon cap and grow backward, in a direction orthogonal to the margin (i.e., parallel to the motion of the silicon). They define radial networks with low sinuosity values. This organization reflects the general direction of the water flow at the silicon/substratum interface and is correlated with the direction of the silicon flow. Similarly, most natural tunnel valleys form at glacial margins and are parallel to ice flow [*Huuse and Lykke-Andersen,* 2000; *van der Vegt et al.,* 2012].
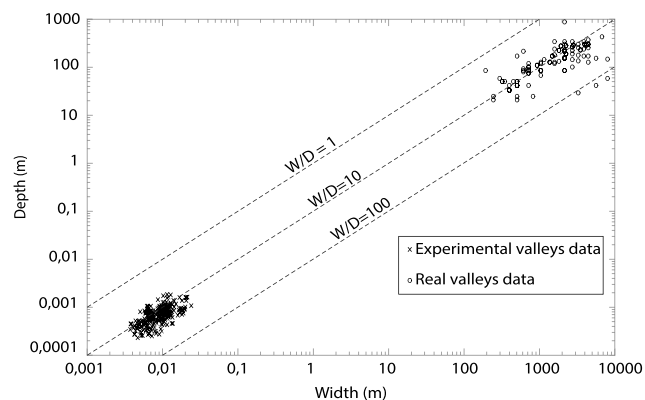

Figure 10. Width-depth ratios for experimental and natural tunnel valleys. References for the natural valleys are given in the supporting information.
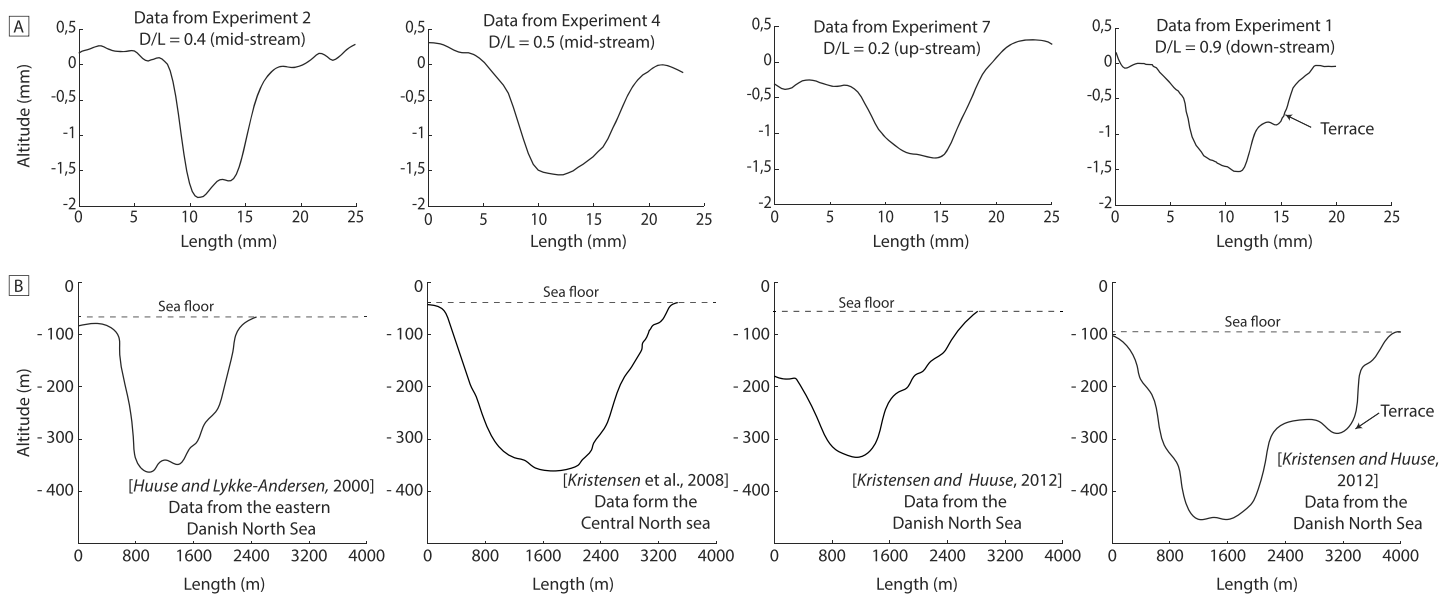
Figure 11. Transverse profiles of selected (a) experimental and (b) natural tunnel valleys. Same vertical exaggeration (x7) for all profiles. D/L: ratio between distance from valley head to displayed profile and total valley length.

These characteristics may be explained by the facts that (1) tunnel valleys initiate preferentially at places where the ice is sufficiently thin that the subglacial water pressure exceeds the sum of the glaciostatic and lithostatic pressure [*Boulton et al.,* 1995] and (2) both ice and subglacial water flow directions are primarily controlled by the surface slope of glaciers [*Paterson*, 1994].

In some experiments, several generations of tunnel valleys have formed as the margin of the silicon cap migrated forward. These successive generations define different networks that have or have not interacted with each other and that may display crosscutting relationships (Figure 8). In all instances, the valleys comprising these networks were orthogonal to the silicon cap margin when they formed, although the orthogonality may have been lost later in response to the motion of the margin. This supports the interpretation that successive generations of tunnel valleys may develop with differing spatial organizations, during successive ice sheet advances and retreats [*Praeg*, 2003; *Sandersen et al.,* 2009].

5.4. Relations Between Tunnel Valley Formation and Ice Velocity

The silicon cap shows, in some experiments, evidence of accelerated flow that resembles surging and ice-streaming events observed in certain glaciers. In the experiments, these "silicon surges" occur in corridors located at the same place as the valleys, and at the same time as the valleys form. These surges appear when the silicon cap is decoupled from the bed by a pressurized water film that decreases the basal friction and therefore accelerates the motion of the silicon (Figure 8b). This result is consistent with the hypothesis that surges in temperate and polythermal glaciers occur in response to pulses of pressurized subglacial meltwater [*Kjær et al.,* 2006] and may be associated with the formation of tunnel valleys. Indeed, many tunnel valleys have been found in the pathway of ice-streams worldwide [*Paterson*, 1994; *Ravier et al.,* 2015]. In glacial systems, subglacial water content, fluid pressure, and basal sliding rate are closely linked [*Harper et al.,* 2007; *Le Brocq et al.,* 2009]. Hence, high meltwater pressures at the interface or within the substratum have been proposed to explain ice-stream mechanisms [*Bennett*, 2003].

5.5. Implications for Tunnel Valley Formation Processes and Timing

Although our experiments do not embrace all the complexity of glacial systems, they produce drainage landforms with shapes and spatial organizations similar to those of natural tunnel valleys. In the experiments, the formation of the valleys results from the development of fluid overpressures in the substratum and at the interface with the silicon cap. This result is consistent with the hypothesis that overpressurized subglacial water controls the formation of tunnel valleys [*Ó Cofaigh,* 1996; *Beaney*, 2002; *van der Vegt et al.,* 2012]. In our experiments, a simple apparatus with a porous and permeable substratum covered by silicon putty was

sufficient to recreate overpressure and initiate "tunnel-like" valleys formation. In nature, however, parameters controlling the development of fluid overpressures are more complex because they include substratum layering, the presence or absence of a subglacial to proglacial permafrost, the topography, the ice thickness, and the meltwater production rate.

Experiments led with a temporal increasing discharge give the opportunity to explore tunnel valley formation under increasing meltwater production rates. A significant increase of discharge can simulate conditions occurring subglacially during an episode of deglaciation. Our first tests have shown that an increase of the water discharge leads to an increase of the erosion rate and thus of tunnel valley dimensions (width and depth). These experimental results possibly imply that tunnel valleys principally acquire their final morphologies and dimensions during deglaciation episodes [*Ó Cofaigh,* 1996; *Praeg,* 2003; *Sandersen et al.,* 2009; *Ravier et al.,* 2015].

6. Conclusions and Future Perspectives

We simulated subglacial water flow by triggering overpressurized water circulation in a permeable and erodible substratum covered by an impermeable, viscous, and transparent cap. The drainage features produced in this way are similar in shape and spatial organization to natural tunnel valleys. The behavior of the silicon cap during experimental tunnel valley development also provides some information on a link between tunnel valley formation and ice flow speed up, such as ice streaming or surging events. Our experimental results are consistent with the hypothesis that overpressurized subglacial water circulation is a key parameter for the development of tunnel valleys. The development of subglacial overpressures is still poorly constrained, however, because it depends on the interplay between the substratum properties (porosity, permeability, erodability, and layering), the ice sheet configuration (thickness, geometry, presence, or absence of a marginal permafrost), and the meltwater production rate. Our experimental apparatus gives us the opportunity to test the impact of these different parameters by modifying the silicon cap geometry, the substratum properties, and the water injection scenario. In addition, the temporal evolution of tunnel valleys and their relationships with the ice dynamics will be investigated further using this new experimental apparatus.

References

Al Hseinat, M., and C. Hübscher (2014), Ice-load induced tectonics controlled tunnel valley evolution—Instances from the southwestern Baltic Sea, *Quat. Sci. Rev.*, *97*, 121–135, doi:10.1016/j.quascirev.2014.05.011.

Atkinson, N., L. D. Andriashek, and S. R. Slattery (2013), Morphological analysis and evolution of buried tunnel valleys in northeast Alberta, Canada, *Quat. Sci. Rev.*, *65*, 53–72, doi:10.1016/j.quascirev.2012.11.031.

Beaney, C. L. (2002), Tunnel channels in southeast Alberta, Canada, *Quat. Int.*, *90*(1), 67–74, doi:10.1016/S1040-6182(01)00093-3.

Bennett, M. R. (2003), Ice streams as the arteries of an ice sheet: Their mechanics, stability and significance, *Earth Sci. Rev.*, *61*(3–4), 309–339, doi:10.1016/S0012-8252(02)00130-7.

Bennett, M. R., D. Huddart, and G. S. P. Thomas (2002), Facies architecture within a regional glaciolacustrine basin: Copper River, Alaska, *Quat. Sci. Rev.*, *21*(20), 2237–2279, doi:10.1016/S0277-3791(02)00027-6.

Bense, V. F., and M. A. Person (2008), Transient hydrodynamics within intercratonic sedimentary basins during glacial cycles, *J. Geophys. Res.*, *113*, F04005, doi:10.1029/2007JF000969.

Björnsson, H., F. Pálsson, O. Sigurðsson, and G. E. Flowers (2003), Surges of glaciers in Iceland, *Ann. Glaciol.*, *36*(1), 82–90.

Blanckaert, K. (2010), Topographic steering, flow recirculation, velocity redistribution, and bed topography in sharp meander bends, *Water Resour. Res.*, *46*, W09506, doi:10.1029/2009WR008303.

Boulton, G. S., and R. C. A. Hindmarsh (1987), Sediment deformation beneath glaciers: Rheology and geological consequences, *J. Geophys. Res.*, *92*(B9), 9059–9082, doi:10.1029/JB092iB09p09059.

Boulton, G. S., T. Slot, K. Blessing, P. Glasbergen, T. Leijnse, and K. van Gijssel (1993), Deep circulation of groundwater in overpressed subglacial aquifers and its geological consequences, *Quat. Sci. Rev.*, *12*(9), 739–745, doi:10.1016/0277-3791(93)90014-D.

Boulton, G. S., P. E. Caban, and K. Van Gijssel (1995), Groundwater flow beneath ice sheets: Part I—Large scale patterns, *Quat. Sci. Rev.*, *14*(6), 545–562, doi:10.1016/0277-3791(95)00039-R.

Boulton, G. S., R. Lunn, P. Vidstrand, and S. Zatsepin (2007), Subglacial drainage by groundwater–channel coupling, and the origin of esker systems: Part II—Theory and simulation of a modern system, *Quat. Sci. Rev.*, *26*(7–8), 1091–1105, doi:10.1016/j.quascirev.2007.01.006.

Breemer, C. W., P. U. Clark, and R. Haggerty (2002), Modeling the subglacial hydrology of the late Pleistocene Lake Michigan Lobe, Laurentide Ice Sheet, *Geol. Soc. Am. Bull.*, *114*(6), 665–674, doi:10.1130/0016-7606(2002)114<0665:MTSHOT>2.0.CO;2.

Carr, M. H., and J. W. Head (2003), Basal melting of snow on early Mars: A possible origin of some valley networks, *Geophys. Res. Lett.*, *30*(24), 2245, doi:10.1029/2003GL018575.

Catania, G., and C. Paola (2001), Braiding under glass, *Geology*, *29*(3), 259–262, doi:10.1130/0091-7613(2001)029<0259:BUG>2.0.CO;2.

Clark, P. U., and J. S. Walder (1994), Subglacial drainage, eskers, and deforming beds beneath the Laurentide and Eurasian ice sheets, *Geol. Soc. Am. Bull.*, *106*(2), 304–314, doi:10.1130/0016-7606(1994)106<0304:SDEADB>2.3.CO;2.

Clerc, S., J.-F. Buoncristiani, M. Guiraud, E. Vennin, G. Desaubliaux, and E. Portier (2013), Subglacial to proglacial depositional environments in an Ordovician glacial tunnel valley, Alnif, Morocco, *Palaeogeogr. Palaeoclimatol. Palaeoecol.*, *370*, 127–144, doi:10.1016/j.palaeo.2012.12.002.

Ó Cofaigh, C. (1996), Tunnel valley genesis, *Prog. Phys. Geogr.*, *20*(1), 1–19, doi:10.1177/030913339602000101.

Domack, E., D. Amblàs, R. Gilbert, S. Brachfeld, A. Camerlenghi, M. Rebesco, M. Canals, and R. Urgeles (2006), Subglacial morphology and glacial evolution of the Palmer deep outlet system, Antarctic Peninsula, *Geomorphology*, *75*(1–2), 125–142, doi:10.1016/j.geomorph.2004.06.013.

Douillet, G., J.-F. Ghienne, Y. Géraud, A. Abueladas, M. Diraison, and A. Al-Zoubi (2012), Late Ordovician tunnel valleys in southern Jordan, *Geol. Soc. London, Spec. Publ.*, *368*(1), 275–292, doi:10.1144/SP368.4.

Dowdeswell, J. A., G. S. Hamilton, and J. O. Hagen (1991), The duration of the active phase on surge-type glaciers: Contrasts between Svalbard and other regions, *J. Glaciol.*, *37*(127), 388–400.

Ehlers, J., and G. Linke (1989), The origin of deep buried channels of Elsterian age in Northwest Germany, *J. Quat. Sci.*, *4*(3), 255–265, doi:10.1002/jqs.3390040306.

Eyles, N., and P. de Broekert (2001), Glacial tunnel valleys in the Eastern Goldfields of Western Australia cut below the Late Paleozoic Pilbara ice sheet, *Palaeogeogr. Palaeoclimatol. Palaeoecol.*, *171*(1–2), 29–40, doi:10.1016/S0031-0182(01)00265-6.

Feurer, D., J.-S. Bailly, C. Puech, Y. Le Coarer, and A. A. Viau (2008), Very-high-resolution mapping of river-immersed topography by remote sensing, *Prog. Phys. Geogr.*, *32*(4), 403–419, doi:10.1177/0309133308096030.

Fisher, T. G., H. M. Jol, and A. M. Boudreau (2005), Saginaw Lobe tunnel channels (Laurentide Ice Sheet) and their significance in south-central Michigan, USA, *Quat. Sci. Rev.*, *24*(22), 2375–2391, doi:10.1016/j.quascirev.2004.11.019.

Flowers, G. E. (2015), Modelling water flow under glaciers and ice sheets, *Proc. R. Soc. A Math. Phys. Eng. Sci.*, vol. *471*(2176), doi:10.1016/j.jappgeo.2003.08.005.

Fountain, A. G., and J. S. Walder (1998), Water flow through temperate glaciers, *Rev. Geophys.*, *36*(3), 299–328, doi:10.1029/97RG03579.

Gabriel, G., R. Kirsch, B. Siemon, and H. Wiederhold (2003), Geophysical investigation of buried Pleistocene subglacial valleys in Northern Germany, *J. Appl. Geophys.*, *53*(4), 159–180, doi:10.1016/j.jappgeo.2003.08.005.

Ghienne, J. F., and M. Deynoux (1998), Large-scale channel fill structures in Late Ordovician glacial deposits in Mauritania, western Sahara, *Sediment. Geol.*, *119*(1–2), 141–159, doi:10.1016/S0037-0738(98)00045-1.

Gibling, M. R. (2006), Width and thickness of fluvial channel bodies and valley fills in the geological record: A literature compilation and classification, *J. Sediment. Res.*, *76*(5), 731–770.

Gooch, B. T., D. A. Young, and D. D. Blankenship (2016), Potential groundwater and heterogeneous heat source contributions to ice sheet dynamics in critical submarine basins of East Antarctica, *Geochem. Geophys. Geosyst.*, *17*, 395–409, doi:10.1002/2015GC006117.

Graveleau, F., and S. Dominguez (2008), Analogue modelling of the interaction between tectonics, erosion and sedimentation in foreland thrust belts, *Comptes Rendus Geosci.*, *340*(5), 324–333, doi:10.1016/j.crte.2008.01.005.

Grube, F. (1983), Tunnel valleys, in *Glacial Deposits in North-west Europe*, pp. 257–258, Balkema, Rotterdam.

Guidat, T., S. Pochat, O. Bourgeois, and O. Souček (2015), Landform assemblage in Isidis Planitia, Mars: Evidence for a 3 Ga old polythermal ice sheet, *Earth Planet. Sci. Lett.*, *411*, 253–267, doi:10.1016/j.epsl.2014.12.002.

Harper, J. T., N. F. Humphrey, W. T. Pfeffer, and B. Lazar (2007), Two modes of accelerated glacier sliding related to water, *Geophys. Res. Lett.*, *34*, L12503, doi:10.1029/2007GL030233.

Head, J. W., and S. Pratt (2001), Extensive Hesperian-aged south polar ice sheet on Mars: Evidence for massive melting and retreat, and lateral flow and ponding of meltwater, *J. Geophys. Res.*, *106*(E6), 12,275–12,299, doi:10.1029/2000JE001359.

Hepp, D. A., D. Hebbeln, S. Kreiter, H. Keil, C. Bathmann, J. Ehlers, and T. Mörz (2012), An east–west-trending Quaternary tunnel valley in the south-eastern North Sea and its seismic–sedimentological interpretation, *J. Quat. Sci.*, *27*(8), 844–853, doi:10.1002/jqs.2599.

Hooke, R. L., and C. E. Jennings (2006), On the formation of the tunnel valleys of the southern Laurentide ice sheet, *Quat. Sci. Rev.*, *25*(11–12), 1364–1372, doi:10.1016/j.quascirev.2006.01.018.

Høyer, A.-S., F. Jørgensen, N. Foged, X. He, and A. V. Christiansen (2015), Three-dimensional geological modelling of AEM resistivity data—A comparison of three methods, *J. Appl. Geophys.*, *115*, 65–78, doi:10.1016/j.jappgeo.2015.02.005.

Huuse, M., and H. Lykke-Andersen (2000), Overdeepened Quaternary valleys in the eastern Danish North Sea: Morphology and origin, *Quat. Sci. Rev.*, *19*(12), 1233–1253, doi:10.1016/S0277-3791(99)00103-1.

Janszen, A., M. Spaak, and A. Moscariello (2012), Effects of the substratum on the formation of glacial tunnel valleys: An example from the Middle Pleistocene of the southern North Sea Basin, *Boreas*, *41*(4), 629–643, doi:10.1111/j.1502-3885.2012.00260.x.

Jentzsch, A. (1884), Über die Bildung der preussischen Seeen, *Zeitschrift der Dtsch. Geol. Gesellschaft*, *36*(3), 699–702.

Jørgensen, F., and P. B. E. Sandersen (2006), Buried and open tunnel valleys in Denmark—Erosion beneath multiple ice sheets, *Quat. Sci. Rev.*, *25*(11–12), 1339–1363, doi:10.1016/j.quascirev.2005.11.006.

Jørgensen, F., H. Lykke-Andersen, P. B. E. Sandersen, E. Auken, and E. Nørmark (2003), Geophysical investigations of buried Quaternary valleys in Denmark: An integrated application of transient electromagnetic soundings, reflection seismic surveys and exploratory drillings, *J. Appl. Geophys.*, *53*(4), 215–228, doi:10.1016/j.jappgeo.2003.08.017.

Kargel, J. S., and R. G. Strom (1992), Ancient glaciation on Mars, *Geology*, *20*, 3, doi:10.1130/0091-7613(1992)020<0003:AGOM>2.3.CO;2.

Kehew, A. E., S. K. Ewald, J. M. Esch, and A. L. Kozlowski (2013), On the origin of tunnel valleys of the Saginaw Lobe of the Laurentide Ice Sheet; Michigan, USA, *Boreas*, *42*(2), 442–462, doi:10.1111/j.1502-3885.2012.00295.x.

Kjær, K. H., E. Larsen, J. van der Meer, Ó. Ingólfsson, J. Krüger, Í. Ö. Benediktsson, C. G. Knudsen, and A. Schomacker (2006), Subglacial decoupling at the sediment/bedrock interface: A new mechanism for rapid flowing ice, *Quat. Sci. Rev.*, *25*(21–22), 2704–2712.

Kluiving, S. J., J. H. Aleid Bosch, H. H. J. Ebbing, C. S. Mesdag, and R. S. Westerhoff (2003), Onshore and offshore seismic and lithostratigraphic analysis of a deeply incised Quaternary buried valley system in the Northern Netherlands, *J. Appl. Geophys.*, *53*(4), 249–271, doi:10.1016/j.jappgeo.2003.08.002.

Kozlowski, A. L., A. E. Kehew, and B. C. Bird (2005), Outburst flood origin of the Central Kalamazoo River Valley, Michigan, USA, *Quat. Sci. Rev.*, *24*(22), 2354–2374, doi:10.1016/j.quascirev.2005.03.016.

Kristensen, T. B., M. Huuse, J. A. Piotrowski, and O. R. Clausen (2007), A morphometric analysis of tunnel valleys in the eastern North Sea based on 3D seismic data, *J. Quat. Sci.*, *22*(8), 801–815, doi:10.1002/jqs.1123.

Kristensen, T. B., J. A. Piotrowski, M. Huuse, O. R. Clausen, and L. Hamberg (2008), Time-transgressive tunnel valley formation indicated by infill sediment structure, North Sea—The role of glaciohydraulic supercooling, *Earth Surf. Process. Landforms*, *33*(4), 546–559, doi:10.1002/esp.1668.

Krohn, C. F., N. K. Larsen, C. Kronborg, O. B. Nielsen, and K. L. Knudsen (2009), Litho- and chronostratigraphy of the Late Weichselian in Vendsyssel, northern Denmark, with special emphasis on tunnel-valley infill in relation to a receding ice margin, *Boreas*, doi:10.1111/j.1502-3885.2009.00104.xr2009.

Latrubesse, E. M. (2015), Large rivers, megafans and other Quaternary avulsive fluvial systems: A potential "who's who" in the geological record, *Earth Sci. Rev.*, *146*, 1–30, doi:10.1016/j.earscirev.2015.03.004.

Le Brocq, A. M., A. J. Payne, M. J. Siegert, and R. B. Alley (2009), A subglacial water-flow model for West Antarctica, *J. Glaciol.*, *55*(193).

Le Heron, D. P. (2007), Late Ordovician glacial record of the Anti-Atlas, Morocco, *Sediment. Geol.*, *201*(1–2), 93–110, doi:10.1016/j. sedgeo.2007.05.004.

Le Heron, D., O. Sutcliffe, K. Bourgig, J. Craig, C. Visentin, and R. Whittington (2004), Sedimentary architecture of Upper Ordovician tunnel valleys, Gargaf Arch, Libya: Implications for the genesis of a hydrocarbon reservoir, *Geoarabia-Manama*, *9*, 137–160.

Lemieux, J.-M., E. A. Sudicky, W. R. Peltier, and L. Tarasov (2008), Simulating the impact of glaciations on continental groundwater flow systems: 1. Relevant processes and model formulation, *J. Geophys. Res.*, *113*, F03017, doi:10.1029/2007JF000928.

Livingstone, S. J., and C. D. Clark (2016), Morphological properties of tunnel valleys of the southern sector of the Laurentide Ice Sheet and implications for their formation, *Earth Surf. Dyn.*, *4*, 567–589, doi:10.5194/esurf-4-567-2016.

Lonergan, L., S. C. R. Maidment, and J. S. Collier (2006), Pleistocene subglacial tunnel valleys in the central North Sea basin: 3-D morphology and evolution, *J. Quat. Sci.*, *21*(8), 891–903, doi:10.1002/jqs.1015.

Lowe, A. L., and J. B. Anderson (2003), Evidence for abundant subglacial meltwater beneath the paleo-ice sheet in Pine Island Bay, Antarctica, *J. Glaciol.*, *49*(164), 125–138, doi:10.3189/172756503781830971.

MacRae, R. A., A. R. Christians, and K. Gajewski (2013), A reexamination of Pleistocene tunnel valley distribution on the central Scotian Shelf, *Can. J. Earth Sci.*, *50*(5), 535–544.

Marczinek, S., and J. A. Piotrowski (2006), Groundwater flow under the margin of the last Scandinavian ice Sheet Around the Eckernföröde Bay, Northwest Germany, in *Glacier Science and Environmental Change*, edited by P. G. Knight, Blackwell, Malden, Mass., doi:10.1002/9780470750636.ch10.

Marra, W. A., E. Hauber, S. J. McLelland, B. J. Murphy, D. R. Parsons, S. J. Conway, M. Roda, R. Govers, and M. G. Kleinhans (2014), Pressurized groundwater outflow experiments and numerical modeling for outflow channels on Mars, *J. Geophys. Res. Planets*, *119*, 2668–2693, doi:10.1002/2014JE004701.

McCabe, A. M., and C. ÓCofaigh (1994), Sedimentation in a subglacial lake, Enniskerry, eastern Ireland, *Sediment. Geol.*, *91*(1–4), 57–95, doi:10.1016/0037-0738(94)90123-6.

Moeller, C. A., D. M. Mickelson, M. P. Anderson, and C. Winguth (2007), Groundwater flow beneath Late Weichselian glacier ice in Nordfjord, Norway, *J. Glaciol.*, *53*(180).

Moores, H. D. (1989), On the formation of the tunnel valleys of the Superior lobe, central Minnesota, *Quat. Res.*, *32*(1), 24–35, doi:10.1016/0033-5894(89)90029-X.

Moreau, J., M. Huuse, A. Janszen, P. van Der Vegt, P. L. Gibbard, and A. Moscariello (2012), The glaciogenic unconformity of the southern North Sea, *Geol. Soc. London, Spec. Publ.*, *368*(1), 99–110, doi:10.1144/SP368.5.

Nye, J. F., and F. C. Frank (1973), Hydrology of the intergranular veins in a temperate glacier, Proceedings of the symposium on hydrology of glaciers, Cambridge.

Parsons, D. R., J. L. Best, S. N. Lane, R. A. Kostaschuk, R. J. Hardy, O. Orfeo, M. L. Amsler, and R. N. Szupiany (2008), Large river channel confluences, in *River Confluences, Tributaries and the Fluvial Network*, edited by S. P. Rice, A. G. Roy, and B. L. Rhoads, John Wiley, Chichester, U. K., doi: 10.1002/9780470760383.ch5.

Paterson, W. S. B. (1994), *The Physics of Glaciers*, Butterwoth-Heinemann, Oxford, U. K.

Person, M., V. Bense, D. Cohen, and A. Banerjee (2012), Models of ice-sheet hydrogeologic interactions: A review, *Geofluids*, *12*(1), 58–78, doi:10.1111/j.1468-8123.2011.00360.x.

Piotrowski, J. A. (1994), Tunnel-valley formation in northwest Germany—Geology, mechanisms of formation and subglacial bed conditions for the Bornhöved tunnel valley, *Sediment. Geol.*, *89*(1–2), 107–141, doi:10.1016/0037-0738(94)90086-8.

Piotrowski, J. A. (1997), Subglacial groundwater flow during the last glaciation in northwestern Germany, *Sediment. Geol.*, *111*(1–4), 217–224, doi:10.1016/S0037-0738(97)00002-X.

Piotrowski, J. A., and S. Tulaczyk (1999), Subglacial conditions under the last ice sheet in northwest Germany: Ice-bed separation and enhanced basal sliding? *Quat. Sci. Rev.*, *18*(6), 737–751, doi:10.1016/S0277-3791(98)00042-0.

Piotrowski, J. A., P. Hermanowski, and A. M. Piechota (2009), Meltwater discharge through the subglacial bed and its land-forming consequences from numerical experiments in the Polish lowland during the last glaciation, *Earth Surf. Process. Landforms*, *34*(4), 481–492, doi:10.1002/esp.1728.

Praeg, D. (2003), Seismic imaging of mid-Pleistocene tunnel-valleys in the North Sea Basin—High resolution from low frequencies, *J. Appl. Geophys.*, *53*(4), 273–298, doi:10.1016/j.jappgeo.2003.08.001.

Rains, R. B., J. Shaw, D. B. Sjogren, M. J. Munro-Stasiuk, K. Robert Skoye, R. R. Young, and R. T. Thompson (2002), Subglacial tunnel channels, Porcupine Hills, southwest Alberta, Canada, *Quat. Int.*, *90*(1), 57–65, doi:10.1016/S1040-6182(01)00092-1.

Ravier, E., J.-F. Buoncristiani, M. Guiraud, J. Menzies, S. Clerc, E. Goupy, and E. Portier (2014), Porewater pressure control on subglacial soft sediment remobilization and tunnel valley formation: A case study from the Alnif tunnel valley (Morocco), *Sediment. Geol.*, *304*, 71–95, doi:10.1016/j.sedgeo.2014.02.005.

Ravier, E., J.-F. Buoncristiani, J. Menzies, M. Guiraud, S. Clerc, and E. Portier (2015), Does porewater or meltwater control tunnel valley genesis? Case studies from the Hirnantian of Morocco, *Palaeogeogr. Palaeoclimatol. Palaeoecol.*, *418*, 359–376, doi:10.1016/j.palaeo.2014.12.003.

Röthlisberger, H. (1972), Water pressure in intra- and subglacial channels*, *J. Glaciol.*, *11*(62).

Russell, H. A., R. W. Arnott, and D. Sharpe (2003), Evidence for rapid sedimentation in a tunnel channel, Oak Ridges Moraine, southern Ontario, Canada, *Sediment. Geol.*, *160*(1–3), 33–55, doi:10.1016/S0037-0738(02)00335-4.

Salcher, B. C., R. Hinsch, and M. Wagreich (2010), High-resolution mapping of glacial landforms in the North Alpine Foreland, Austria, *Geomorphology*, *122*(3–4), 283–293, doi:10.1016/j.geomorph.2009.09.037.

Sandersen, P. B. E., and F. Jørgensen (2012), Substratum control on tunnel-valley formation in Denmark, *Geol. Soc. London Spec. Publ.*, *368*(1), 145–157, doi:10.1144/SP368.12.

Sandersen, P. B. E., F. Jørgensen, N. K. Larsen, J. H. Westergaard, and E. Auken (2009), Rapid tunnel-valley formation beneath the receding Late Weichselian ice sheet in Vendsyssel, Denmark, *Boreas*, *38*(4), 834–851, doi:10.1111/j.1502-3885.2009.00105.x.

Shaw, J. (2002), The meltwater hypothesis for subglacial bedforms, *Quat. Int.*, *90*(1), 5–22, doi:10.1016/S1040-6182(01)00089-1.

Shaw, J. (2010), In defence of the meltwater (megaflood) hypothesis for the formation of subglacial bedform fields, *J. Quat. Sci.*, *25*(3), 249–260, doi:10.1002/jqs.1264.

Sjogren, D. B., and R. B. Rains (1995), Glaciofluvial erosional morphology and sediments of the Coronation–Spondin Scabland, east-central Alberta, *Can. J. Earth Sci.*, *32*(5), 565–578, doi:10.1139/e95-048.

Smith, J. A., C.-D. Hillenbrand, R. D. Larter, A. G. C. Graham, and G. Kuhn (2009), The sediment infill of subglacial meltwater channels on the West Antarctic continental shelf, *Quat. Res.*, *71*(2), 190–200, doi:10.1016/j.yqres.2008.11.005.

Solomina, O. N., et al. (2016), Glacier fluctuations during the past 2000 years, *Quat. Sci. Rev.*, *149*, 61–90, doi:10.1016/j.quascirev.2016.04.008.

Souček, O., O. Bourgeois, S. Pochat, and T. Guidat (2015), A 3 Ga old polythermal ice sheet in Isidis Planitia, Mars: Dynamics and thermal regime inferred from numerical modeling, *Earth Planet. Sci. Lett.*, *426*, 176–190, doi:10.1016/j.epsl.2015.06.038.

Stewart, M. A., and L. Lonergan (2011), Seven glacial cycles in the middle-late Pleistocene of northwest Europe: Geomorphic evidence from buried tunnel valleys, *Geology*, *39*(3), 283–286, doi:10.1130/G31631.1.

Stewart, M. A., L. Lonergan, and G. Hampson (2013), 3D seismic analysis of buried tunnel valleys in the central North Sea: Morphology, cross-cutting generations and glacial history, *Quat. Sci. Rev.*, *72*, 1–17, doi:10.1016/j.quascirev.2013.03.016.

Thomas, R. H., S. N. Stephenson, R. A. Bindschadler, S. Shabtaie, and C. R. Bentley (1988), Thinning and grounding-line retreat on Ross Ice Shelf, Antarctica, *Ann. Glaciol.*, *11*, 165–172.

Tournier, F., M. Pagel, E. Portier, I. Wazir, and N. Fiet (2010), Relationship between deep diagenetic quartz cementation and sedimentary facies in a Late Ordovician glacial environment (Sbaa Basin, Algeria), *J. Sediment. Res.*, *80*(12), 1068–1084, doi:10.2110/jsr.2010.094.

van der Vegt, P., A. Janszen, and A. Moscariello (2012), Tunnel valleys: Current knowledge and future perspectives, *Geol. Soc. London Spec. Publ.*, *368*(1), 75–97, doi:10.1144/SP368.13.

Van Dijke, J. J., and A. Veldkamp (1996), Climate-controlled glacial erosion in the unconsolidated sediments of northwestern Europe, based on a genetic model for tunnel valley formation, *Earth Surf. Process. Landforms*, *21*(4), 327–340, doi:10.1002/(SICI)1096-9837(199604)21:4<327::AID-ESP540>3.0.CO;2-P.

Wingfield, R. (1990), The origin of major incisions within the Pleistocene deposits of the North Sea, *Mar. Geol.*, *91*(1–2), 31–52, doi:10.1016/0025-3227(90)90131-3.

Winsemann, J., U. Asprion, T. Meyer, and C. Schramm (2007), Facies characteristics of Middle Pleistocene (Saalian) ice-margin subaqueous fan and delta deposits, glacial Lake Leine, NW Germany, *Sediment. Geol.*, *193*(1), 105–129, doi:10.1016/j.sedgeo.2005.11.027.

Woodland, A. W. (1970), The buried tunnel-valleys of East Anglia, in *Proceedings of the Yorkshire Geological and Polytechnic Society*, vol. 37, pp. 521–578, doi:10.1144/pygs.37.4.521.